Macromolecules

ARTICLE

pubs.acs.org/Macromolecules

Melting and van der Waals Stabilization of PE Single Crystals Grown from Ultrathin Films

Fajun Zhang,*[,†] Gabriel G. Baralia,[‡,§] Bernard Nysten,[‡] and Alain M. Jonas*[,‡]

[†]Institut für Angewandte Physik, Eberhard Karls Universität Tübingen, Auf der Morgenstelle 10, D-72076 Tübingen, Germany

[‡]Bio & Soft Matter, Institute for Condensed matter and Nanosciences (IMCN), Université catholique de Louvain, Croix du Sud 1, box L7.04.01, B-1348 Louvain-la-Neuve, Belgium

ABSTRACT: We have obtained a series of single- and multilayered extended chain polyethylene (PE) crystals resting on a silicon dioxide substrate by crystallizing a low molar mass oligomer fraction of low polydispersity from an ultrathin film. Crystal thicknesses were determined from the height histograms of atomic force microscopy (AFM) images. For crystallization temperatures above 108 °C, the thickness of each layer was 16.9 ± 1.4 nm, close to the computed average extended length of the oligomer chain. The crystal melting was followed by a hot-stage optical microscopy (OM) in reflection. Different layers melt at different temperatures, due to differences in interfacial free energy depending on whether they are in contact with the substrate or another layer or have a free interface. The interfacial free energies of the different interfaces were obtained by the Gibbs−Thompson equation, and the difference between them was quantitatively related to the van der Waals stabilization energy resulting from placing a layer in contact with the substrate or with another layer. Our study demonstrates the importance of interfaces when considering the thermal behavior of ultrathin films of crystalline polymers and illustrates that a simple energetic concept can be used to explain the stabilization of crystals resting on a surface.

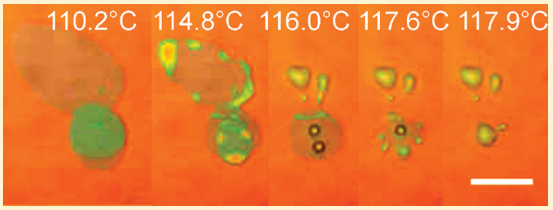

INTRODUCTION

When long-chain polymer macromolecules are confined in ultrathin films of thickness comparable to their radius of gyration, their physical properties may be changed compared with the bulk state because interfaces play an increasing important role in the total free energy of the system.[1] For instance, studies on polymer crystallization in thin and ultrathin films indicate that the growth rate and morphology of the crystals change continuously with decreasing film thickness.[2−27] Usually, a decrease of crystallization rate and crystallinity is reported with decreasing film thickness.[2−9]

The film thickness was also found to affect the melting temperature (T_m) of polymers crystallized in thin films. For instance, Kim et al. found that the T_m of poly(ethylene-*co*-vinyl acetate) films on silicon wafers decreases dramatically when the film thickness is less than 30 nm, under identical crystallization conditions.[5] This was hypothesized to be due to a reduction of crystal thickness in thin films. Indeed, T_m and crystal thickness, l, are reciprocally related as indicated by the well-known Gibbs−Thompson equation[28]

$$T_m = T_m^e\left(1 - \frac{2\sigma}{l\Delta h_f}\right) \quad (1)$$

where T_m^e is the equilibrium melting temperature, σ is the interfacial free energy of the basal interfaces of the crystalline lamellae, and Δh_f is the bulk heat of fusion per unit volume.[28] However, the Gibbs−Thompson equation indicates that other reasons may be responsible for the reduction of T_m, such as a change of the basal surface energy of the crystal σ. This was proposed by Wang et al., who investigated the crystallization of poly(ethylene-*co*-vinyl acetate) and linear low-density polyethylene (PE) in thin and ultrathin films.[6] The melting temperature was also reported to decrease with decreasing thickness for films thinner than 100 nm. However, the measured lamellar thickness, l, increased rather than decreased with decreasing film thickness, implying that a variation of σ was the main reason for the decrease of T_m. This suggests that, in thin films, T_m might be strongly influenced as well by polymer−surface interactions that directly affect the basal surface energy.[6] The questions which arise are then whether the crystal surfaces differ significantly at the different interfaces in thin films and, if so, how these different interfacial structures do affect the final melting behavior of polymer crystals in thin films.

Direct evidence on the difference of interface structures of lamellar crystals formed in thin films was reported by Keith et al.[10] These authors obtained by the polyethylene decoration technique decoration patterns for both air/crystal and crystal/substrate interfaces of lamellar crystals. Interestingly, it was found that the pattern corresponding to the crystal/substrate interface was the reverse of the one of corresponding regions at the air/crystal interface. This observation indicated that the fold structures, and therefore interfacial free energies, of crystal surfaces at air/crystal and crystal/substrate interfaces may differ from

Received: May 30, 2011
Revised: July 22, 2011
Published: September 07, 2011

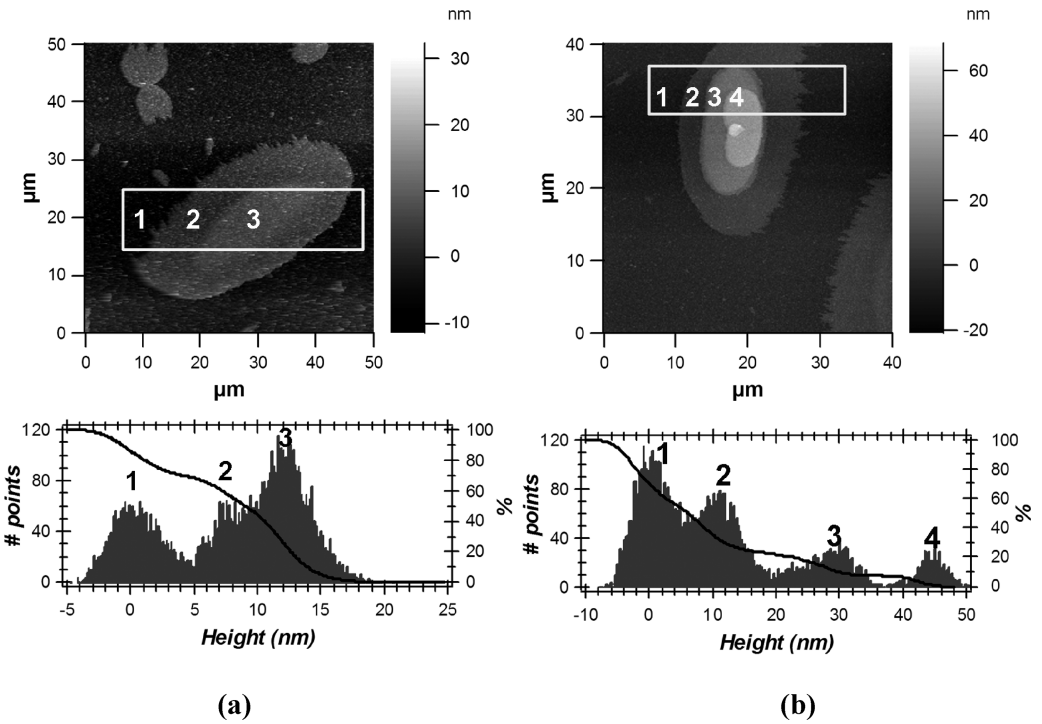

Figure 1. AFM topography images of PE crystals grown at 114.5 °C from an ultrathin film. (a) Single-layer extended-chain crystal, surrounded by a shell of folded crystal grown during quenching. (b) Multilayered extended chain crystals. Height histograms corresponding to white boxes are shown at the bottom. Note that the height of the background containing the residual film (∼5 nm) has been set to zero.

each other. This is in contrast to the study of the crystallization and melting of poly(ethylene oxide) (PEO) on oxidized silicon surfaces[7−9] where the equilibrium melting temperatures of PEO crystals and the surface free energies of the PEO fold surfaces agreed quantitatively with the values obtained for bulk crystallization.

Hence, considering the discrepancies between these different sets of results, it appears that polymer crystals in thin or ultrathin films need further study. Here we report on the effect of interfaces on the melting of polyethylene single crystals formed in ultrathin films. To decrease complexity due to, e.g., the folding process, we work with a low molar mass PE of low polydispersity, which tends to form extended chain crystals. The ultrathin film, of thickness around 5 nm, was formed by the partial dewetting of a PE thin film spin-coated on a rough substrate.[29] Our results indicate that PE single crystals formed in ultrathin films are stabilized by the van der Waals interaction they experience with the substrate, giving rise to higher melting temperatures.

EXPERIMENTAL SECTION

Materials. A polyethylene fraction was obtained from Polymer Laboratories Ltd., UK, with a weight-average molar mass (M_w) of 2155 g mol^{-1} and a polydispersity (M_w/M_n) of 1.14. Its average extended chain length (L_e) is 17.1 nm, calculated from $L_e = (M_n/14.03) \times 0.127$ nm valid for PE in its planar zigzag conformation.[28]

Preparation of Polymer Films by Spin-Coating.[29,30] Silicon wafers with a 260 nm thick dioxide layer prepared by plasma-enhanced chemical vapor deposition (PECVD) were used as substrates and were cleaned by immersion for 20 min in a hot 1:1 vol 98% H_2SO_4:27% H_2O_2 mixture ("piranha solution"; *caution: piranha solution is highly corrosive; extreme care should be taken when handling piranha solution!*) followed by extensive rinsing with ultrapure water (obtained by deionization and purification using the Milli-Q system from Millipore). This procedure efficiently removed organic contaminants without introducing measurable roughening of the surface. The slight roughness of the substrates prevented us from measuring reliably their surface tension. However, experiments performed on flatter piranha-cleaned silicon oxide surfaces provided 43−45 mJ/m^2 for the dispersive component of surface tension and 20−24 mJ/m^2 for its polar component.[31] A PE solution 1.5 wt % in decalin was prepared for spin-coating. Before spin-coating, all equipments, including silicon wafer, polymer solution, holder of spin-coater, pipets, and tweezer, were preheated to 160 °C in an oven close to the spin-coater. The transfer of the hot substrate and solution from oven to spin start took about 10 s. Spin speed was 3000 rpm for 30 s. The resulting film thickness measured by ellipsometry was in the range of 80−90 nm.

Crystallization and Melting. An Olympus AX70 optical microscope equipped with a Mettler Toledo FP82HT hot-stage was used in this work. The temperature was controlled by a Mettler FP90 central processor. Samples covered with a glass slide were first molten at 140 °C and held at this temperature for 1 min; during this procedure, partial dewetting of the molten polymer film occurred quickly, leaving molten droplets on a residual ultrathin polymer film of ∼5 nm average thickness.[29] In the sequel, we concentrate on crystals growing from this residual film, ignoring phenomena occurring in the remaining large droplets randomly dispersed over the residual film. The detailed morphological characterization of the film after partial dewetting is reported elsewhere.[29] The samples were then cooled down to preset crystallization temperatures at −20 °C/min. The crystal morphology was captured at different growth stages by a digital camera. After crystallization for a preset time, the samples were heated immediately at a scan rate of 1.0 °C/min to measure their melting point with a resolution and repeatability of ±0.1 °C or quenched to room temperature for AFM measurements. The absolute precision of the temperature measurement is however lower, since no attempt to calibrate the hot stage with precision was performed. An absolute error of about ∼3 °C is

dx.doi.org/10.1021/ma2012249 |*Macromolecules* 2011, 44, 7752–7757

Scheme 1. Illustration of the Single- and Multilayered Crystals Formed from the Ultrathin Film[a]

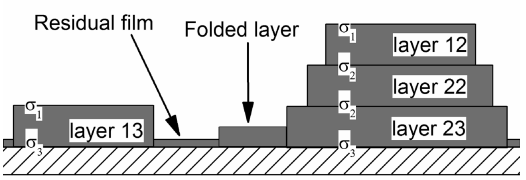

[a] The interfacial free energy of air/crystal, crystal/crystal, and crystal/substrate interfaces is denoted as σ_1, σ_2, and σ_3, respectively.

probable, based on the measurement of the melting temperature of an indium sample.

Atomic Force Microscopy (AFM). Tapping mode AFM experiments were performed at room temperature, with an Autoprobe CP (Park Scientific Instruments). A large size (100 μm × 100 μm) scanner was employed. Images were acquired in tapping mode at a scan rate of 0.35−0.5 Hz with silicon cantilevers. Trace, retrace, and noise images were obtained simultaneously. Processing and analysis of AFM images were performed with homemade programs written in Igor Pro (Wavemetrics, Portland, OR).

RESULTS

Crystal Thickness. Figure 1 shows AFM height images of single or multilayered crystals formed at T_c = 114.5 °C. The samples were quenched to room temperature after crystallization, and AFM measurements were conducted at room temperature. During the quench, a thin crystalline layer crystal formed at the edge of the crystals previously grown at the preset T_c. One example is shown in Figure 1a (layer 2). The sample was quenched to room temperature after crystallization at 114.5 °C for 6 h. In the center of the lamella, an asymmetric lenticular crystal noted 3 can be seen, which appeared at 114.5 °C. Surrounding it, a layer of lower height is visible, corresponding to a crystal which grew during the quench. This is more clearly seen in the histogram of heights of the region delimitated in the AFM image (Figure 1a, bottom), which shows three peaks corresponding to the heights of the background residual film (peak 1), of the thin layer formed during quench (peak 2), and of the crystal formed at 114.5 °C (peak 3). The thin layer formed during the quench and the lenticular crystals protrude from the background by 8 and 12 nm, respectively. Since the thickness of the background residual film is ∼5 nm,[29] this corresponds to a lenticular crystal of ∼17 nm thickness, close to the extended length of our PE chains (L_e =17.1 nm), whereas the crystalline layer formed during the quench is about 13 nm thick. Multilayered crystals were also obtained during crystallization, as shown in Figure 1b, whose height histogram exhibits three additional peaks protruding by 10, 28, and 44 nm over the background peak (which is set to zero). Considering again the ∼5 nm thickness of the residual film, this corresponds to crystals of ∼15, ∼33, and ∼49 nm, which coincides within experimental error with crystals made of 1, 2, and 3 extended chain crystalline layers, respectively.

The structure of these crystalline layers is illustrated in Scheme 1. At least four different types of extended chain crystalline layers should thus be considered, not counting the crystalline layer which also frequently appears during the quench (Scheme 1): the single-layer crystal (layer 13), the top (layer 12), and bottom (layer 23) layers of multilayered crystals and the

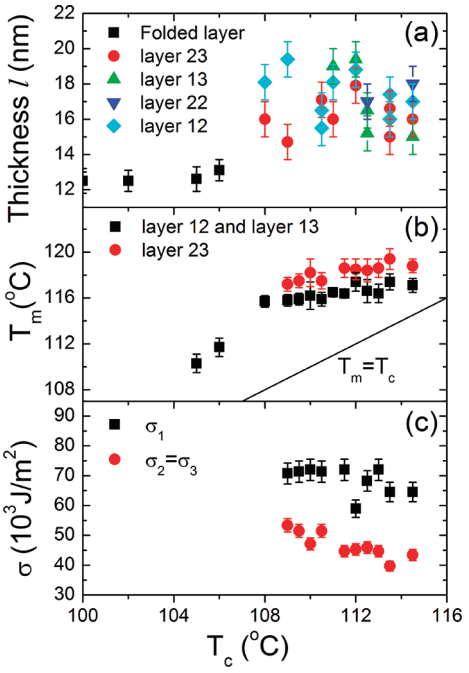

Figure 2. (a) Thickness of the different types of crystalline layers versus crystallization temperature T_c. (b) Melting temperature T_m vs crystallization temperature for the different types of crystalline layers. (c) Interfacial free energy of the different interfaces shown in Scheme 1 as a function of crystallization temperature.

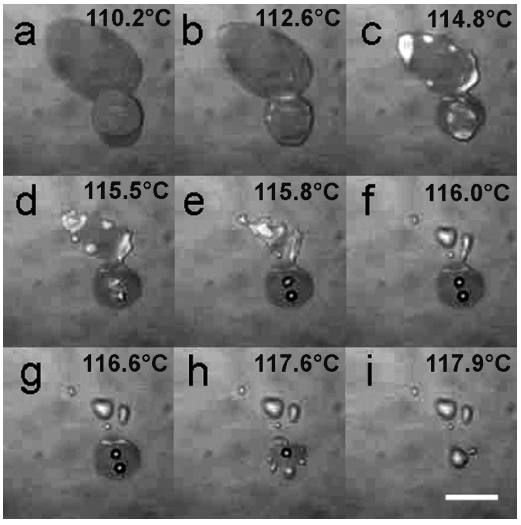

Figure 3. Series of OM images showing the progressive melting of a single- and a double-layer truncated lozenge-shape crystals formed at 110.5 °C (1.0 °C/min heating rate). The temperatures are indicated in the images. The scale bar is 20 μm.

inner layers of multilayered crystals (layer 22). Figure 2a displays the thickness of these different types of crystalline layers versus T_c, measured by AFM from images similar to Figure 1b. When T_c < 106 °C, crystals of 12.5 nm thickness are formed, independent of T_c. These crystals are of a thickness identical to those formed during quenching and consist either of nonintegrally folded chains or more probably of chains tilted with respect to the normal to the substrate. When T_c > 108 °C, extended-chain

dx.doi.org/10.1021/ma2012249 |*Macromolecules* 2011, 44, 7752–7757

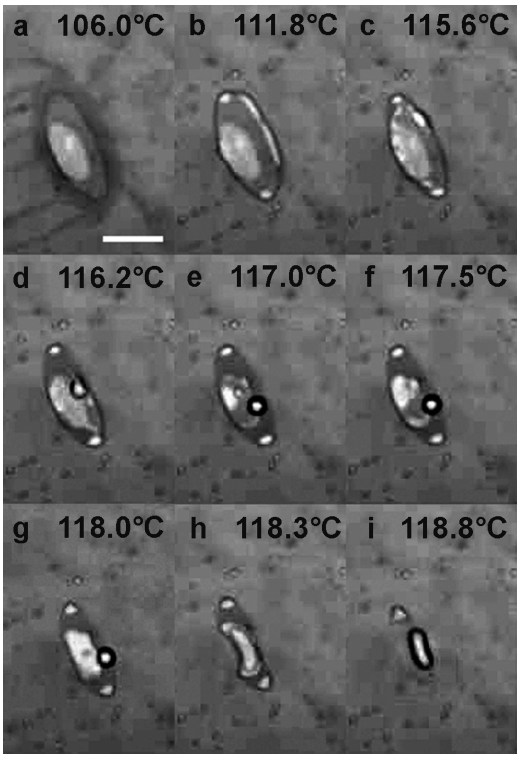

Figure 4. Series of OM images showing the progressive melting of a trilayered crystal formed at 114.5 °C (1.0 °C/min heating rate). The temperatures are indicated in the images. The scale bar is 20 μm.

crystals are formed, which can be single- or multilayered. Considering the uncertainty on the thickness of the bottom-most crystalline layers (layers 13 and 23 in Figure 2b), which results from the uncertainty on the thickness of the residual film, we can safely conclude that all types of extended chain layers are of identical thickness, close to 16.9 ± 1.4 nm based on 24 measurements. This average value is remarkably close to the calculated extended chain length, L_e = 17.1 nm.

Crystal Melting Behavior. Since the external surfaces of each crystalline layers defined in Scheme 1 are in contact with different media, they may have different interface structure and interfacial free energies (denoted as σ_1, σ_2, and σ_3 in Scheme 1) and therefore may melt at different temperatures even though they are of identical thickness. To test this possibility, the melting of the single crystals formed at various temperatures was studied by hot-stage OM under slow heating scan conditions (1.0 °C/min). The melting of single- and double-layered crystals formed at 110.5 °C is shown in Figure 3. The sample was quenched to room temperature before the heating scan, during which consecutive pictures were taken every 0.2−0.3 °C (these pictures are not all shown in Figures 3 and 4). Upon increasing temperature, melting occurs first at the crystal edges below 112.6 °C due to the melting of the thinner crystalline layer which formed during the quench and borders the extended chain crystals. The melting of the single-layered extended chain crystal and of the topmost layer of the double-layered extended chain crystal occurs between 114.8 and 115.8 °C. Meanwhile, the bottom layer of the double-layered crystal is still in the solid state; it finally melts between 116.6 and 117.6 °C. Another example of melting is shown in Figure 4, which illustrates the progressive melting of a trilayered crystal formed at 114.5 °C. The sample was quenched to room temperature before heating. Upon increasing temperature, the thinner crystalline layer resulting from the quench melts at about 111.8 °C as in the previous experiment. The topmost layer of the extended chain crystal then melts in between 116.2 and 117 °C, revealing an intermediate layer below it, which melts at about 118.3 °C. The bottom layer of the trilayered crystal finally melts at 118.8 °C. Most interestingly, as can be seen in the images but was even clearer in the direct observation, the second layer of the crystal melts at 116.2−117 °C in the area not covered by the third layer, whereas it resists melting until 118.3 °C in its area located below the third layer. It is interesting to note that the melt PE droplets dewet the crystalline PE as shown in Figures 3 and 4.

The melting behavior of such single- or multilayered crystals formed at different T_c's in the range 108−114.5 °C was then systematically studied. We always found that the T_m of the bottom-most layer of a multilayered crystal is higher than the T_m of a single-layered crystal, whose T_m is similar to the one of the topmost layer of a multilayered crystal. The melting behavior of intermediate layers in multilayered crystals is more difficult to determine because these layers are frequently covered by melt droplets. However, they usually melt at temperatures close to the T_m of the bottom-most layers of multilayered crystals. Figure 2b presents the T_m's of the different types of layers versus crystallization temperature T_c. The T_m's of the outermost layer of multilayered crystals are generally identical to the T_m's of single-layered crystals, whereas the T_m's of the bottom-most layer of multilayered crystals is on the average 1.8 ± 0.4 °C higher, as determined on a large series of samples. As the melting of intermediate layers was rarely observed, their T_m's are not reported in Figure 2b.

DISCUSSION

Interfacial Free Energy. The simplified Gibbs−Thompson equation (eq 1) describes the relation between the thickness, l, melting temperature, T_m, and interfacial free energy, σ, of the basal planes of lamellar crystals. For our low molecular weight PE fraction, an equilibrium melting temperature T_m^e = 398.9 K is predicted from T_m^e = 414.1 − 2071/x, where x is the average number of carbons in the polymer chain.[28] The DSC-determined experimental melting point of the fraction, determined after crystallization at 117 °C, is 124.8 °C (398.0 K), close to T_m^e, indicating that extended chain crystals are formed. For such extended chain crystals, the modified equation proposed by Flory is usually taken instead of the simplified Gibbs−Thompson equation.[32] However, the Gibbs−Thompson equation can still be used as the interpretative basis for the results displayed in Figure 2. For instance, the slight increase of T_m vs crystallization temperature (Figure 2b) may be ascribed to slight differences in crystal perfection which would affect Δh_f and/or to the entropic component of the interfacial energy, σ. More importantly, this equation indicates that the 1.8 ± 0.4 °C difference between the T_m's of different extended chain crystalline layers (Figure 2b), although they are of identical thickness (Figure 2a), arises from differences in interfacial free energy.

The melting temperatures of the crystals in the thin films by optical microscopy (~118 °C) are significantly lower than the one measured in the bulk by DSC (124.8 °C). This is because the interfacial free energies that have to be taken into account in the Gibbs−Thompson equation are the ones that exist when the crystal starts to melt. In the bulk, the crystal is surrounded by amorphous molten material, whereas the situation is entirely

different in the thin film. Differences in the structure of the crystal−amorphous interfaces are also likely. In addition, because the absolute accuracy of the melting temperatures in the thin films is relatively low, no attempt was performed here to analyze quantitatively the differences of melting temperature between bulk and thin film.

Instead, we focus on the difference of melting temperatures between different crystalline layers in the thin films, for which the accuracy is high. When deriving the Gibbs−Thompson equation, the interfacial energies to take into account are the one of the crystal starting to melt (state 1) and the one of the resulting molten material (state 2). Because the surface of molten polymer droplets is much smaller than the one of the lamellar crystals (Figures 3 and 4), we may safely ignore the interfacial energies of the molten polymer (that is also generally ignored for bulk melting). Using the notations of Scheme 1, eq 1 can be developed for each crystalline layer *ij*:

$$T_m^{ij} = T_m^e\left(1 - \frac{\sigma_i + \sigma_j}{l\Delta h_f}\right) \quad (2)$$

Shown in Figure 2c are the σ_i's computed from this equation and the data of Figure 2b, using $T_m^e = 398.9$ K, $\Delta h_f = 2.93 \times 10^2$ J/cm^3,[28] and $l = 16.9$ nm. The average interfacial free energies are $\sigma_1 = (68 \pm 5) \times 10^{-3}$ J/m^2 and $\sigma_2 = \sigma_3 = (47 \pm 5) \times 10^{-3}$ J/m^2 and decrease slightly with increasing T_c. Because our data have a high relative but a low absolute precision, we concentrate only on the difference $\Delta\sigma_{12} = \sigma_1 - \sigma_2 = (21 \pm 7) \times 10^{-3}$ J/m^2 (also equal to $\Delta\sigma_{13} = \sigma_1 - \sigma_3$). This difference corresponds to the excess surface energy associated with a crystal interface in air or in contact with another crystal (or with the substrate).

Interface Structure and Stabilization. From the interfacial free energy of crystal/air and crystal/crystal interfaces, the average distance between two crystalline layers in contact with each other can be computed (contact plane corresponding to σ_2 in Scheme 1). The surface van der Waals stabilization energy resulting from bringing two planar semi-infinite hydrocarbonaceous bodies from infinity to a distance d is[33]

$$\Delta E = \frac{-A_{PE/PE}}{12\pi d^2} \quad (3)$$

where $A_{PE/PE} = \sim 4.7 \times 10^{-20}$ J is the nonretarded Hamaker constant for two PE semi-infinite bodies interacting across a vacuum, here taken as identical to the Hamaker constant of tetradecane.[34] This equation is also valid for layers of 16.9 nm thickness, provided d is smaller than a few nanometers. This ΔE should thus coincide with the $\sim 20 \times 10^{-3}$ J/m^2 difference between the interfacial free energies measured for the crystal/air and crystal/crystal interfaces, which implies that the average distance between two crystalline layers should be $d \sim 0.25$ nm. Calculation using the Hamaker constant of PE (5.75×10^{-20} J)[35] gives the distance of 0.28 nm, which is consistent with our calculation. This d value can be compared to the intermolecular distance between the terminal C atoms of successive layers in multilayered crystals of *n*-alkanes, which was reported to be ~0.36 nm for *n*-alkanes containing from 6 to 24 C atoms[36] and 0.31 nm for a series of *n*-alkanes crystallized in their orthorhombic, triclinic, or monoclinic modifications.[37] This result thus strongly suggests that, for our extended-chain crystals of polydisperse oligomers, the methyl groups of neighboring layers pack tightly, so that protruding chains of the top layer enter into the holes left by shorter chains of the bottom layer.

Likewise, the average distance between the bottom crystalline layer and the silicon dioxide substrate can be computed from the interfacial free energy of crystal/air and crystal/surface interfaces (contact plane corresponding to σ_3 in Scheme 1). The Hamaker constant for PE interacting with amorphous silicon dioxide through a vacuum may be estimated from spectroscopic data; it amounts to $A_{PE/SiO_2} = \sim 5.5 \times 10^{-20}$ J.[38] From this, the average distance between the bottom crystalline layer and the SiO_2 surface is $d = 0.31$ nm, essentially corresponding to methyl groups being in contact with the surface of the wafer, as expected.

These estimations suggest that the van der Waals interaction is the reason why the surfaces of crystalline layers in contact with the substrate or with another crystalline layer have a lower interfacial free energy than free surfaces. In addition, they support a view where close contact is maximized between adjacent layers or with the substrate, which minimizes "local porosity" and therefore stabilizes the interfaces. This extra-stabilization is responsible for the slightly higher melting temperature observed for the crystalline layers lacking a free interface.

CONCLUSIONS

By crystallizing a PE oligomer fraction from an ultrathin film, we have obtained a series of single- and multilayered extended chain crystals resting on a silicon dioxide substrate. Within experimental precision, the thickness of each layer was measured to be 16.9 ± 1.4 nm, independent of crystallization temperature above 108 °C and in good agreement with the computed average extended length of the oligomer. We have measured the melting temperature of each layers in these single- and multilayered crystals and computed the interfacial free energy of the layers. The difference was quantitatively related to the van der Waals stabilization energy resulting from placing a layer in contact with the substrate or with another layer. The average distance between a layer and the substrate, or between two layers, is in the 0.3 nm range, indicating that the roughness of the substrate and of the layers is followed conformally by the next layer, with holes of a layer or substrate being filled by protrusions of the next layer. The consequence of these differences in interfacial free energy is a lower melting temperature (by ~1.8 ± 0.4 °C) of layers having a free surface (air/layer interface) than layers having no free interface, despite their are of identical thickness and crystallization temperature. Our study thus demonstrates the importance of interfaces when considering the thermal behavior of ultrathin films of crystalline polymers and illustrates that simple energetic concept can be used to quantify the peculiarity of this behavior.

AUTHOR INFORMATION

Corresponding Author

*E-mail: alain.jonas@uclouvain.be (A.M.J.); fajun.zhang@uni-tuebingen.de (F.Z.).

Present Addresses

[§]Carl Zeiss SMS, Industriestrasse 1, D-64380, Rossdorf, Germany.

ACKNOWLEDGMENT

Partial financial support was provided by the Belgium National Science Foundation (FNRS) and the FSR of UCL. The authors thank C. Bailly, A. Boborodea from UCL, and Prof. G. Reiter (University of Freiburg) for valuable discussions.

REFERENCES

(1) *Physics of Polymer Surfaces and Interfaces*; Sanchez, I. C., Ed.; Butterworth-Heinemann: Boston, 1992.

(2) Frank, C. W.; Rao, V.; Despotopoulou, M. M.; Pease, R. F. W.; Hinsberg, W. D.; Miller, R. D.; Rabolt, J. F. *Science* **1996**, *273*, 912.

(3) Despotopoulou, M. M.; Frank, C. W.; Miller, R. D.; Rabolt, J. F. *Macromolecules* **1995**, *28*, 6687.

(4) Despotopoulou, M. M.; Frank, C. W.; Miller, R. D.; Rabolt, J. F. *Macromolecules* **1996**, *29*, 5797.

(5) Kim, J. H.; Jang, J.; Zin, W. *Macromol. Rapid Commun.* **2001**, *22*, 386.

(6) Wang, Y.; Ge, S.; Rafailovich, M.; Sokolov, J.; Zou, Y.; Ade, H.; Luning, J.; Lustiger, A.; Maron, G. *Macromolecules* **2004**, *37*, 3319.

(7) Schönherr, H.; Frank, C. W. *Macromolecules* **2003**, *36*, 1188.

(8) Schönherr, H.; Bailey, L. E.; Frank, C. W. *Langmuir* **2002**, *18*, 490.

(9) Schönherr, H.; Frank, C. W. *Macromolecules* **2003**, *36*, 1199.

(10) Keith, H. D.; Padden, J. F. J.; Lotz, B.; Wittmann, J. C. *Macromolecules* **1989**, *22*, 2230.

(11) Beers, K. L.; Douglas, J. F.; Amis, E. J.; Karim, A. *Langmuir* **2003**, *19*, 3935.

(12) Dalnoki-Veress, K.; Forrest, J. A.; Massa, M. V.; Pratt, A.; Williams, A. *J. Polym. Sci., Part B: Polym. Phys.* **2001**, *39*, 2615.

(13) Godovsky, Y. K.; Magonov, S. N. *Langmuir* **2000**, *16*, 3549.

(14) Li, H.; Yan, S. *Macromolecules* **2011**, *44*, 417.

(15) Liu, Y.-X.; Chen, E.-Q. *Coord. Chem. Rev.* **2010**, *254*, 1011.

(16) Massa, M. V.; Dalnoki-Veress, K.; Forrest, J. A. *Eur. Phys. J. E* **2003**, *11*, 191.

(17) Reiter, G.; Sommer, J. U. *Phys. Rev. Lett.* **1998**, *80*, 3771.

(18) Reiter, G.; Sommer, J. U. *J. Chem. Phys.* **2000**, *112*, 4376.

(19) Salim, O. K.; Levent Demirel, A. *J. Macromol. Sci., Part B: Phys.* **2003**, *B42*, 611.

(20) Sutton, S. J.; Izumi, K.; Miyaji, H.; Miyamoto, Y.; Miyashita, S. *J. Mater. Sci.* **1997**, *32*, 5621.

(21) Taguchi, K.; Miyaji, H.; Izumi, K.; Hoshino, A.; Miyamoto, Y.; Kokawa, R. *Polymer* **2001**, *42*, 7443.

(22) Taguchi, K.; Miyaji, H.; Izumi, K.; Hoshino, A.; Miyamoto, Y.; Kokawa, R. *J. Macromol. Sci., Part B: Phys.* **2002**, *B41*, 1033.

(23) Zhang, F.; Liu, J.; Huang, H.; Du, B.; He, T. *Eur. Phys. J. E* **2002**, *8*, 289.

(24) Xu, J.; Ma, Y.; Hu, W.; Rehahn, M.; Reiter, G. *Nature Mater.* **2009**, *8*, 348.

(25) Jradi, K.; Bistac, S.; Schmitt, M.; Schmatulla, A.; Reiter, G. *Eur. Phys. J. E: Soft Matter Biol. Phys.* **2009**, *29*, 383.

(26) Bi, W.; Teguh, J. S.; Yeow, E. K. L. *Phys. Rev. Lett.* **2009**, *102*, 048302.

(27) *Progress in Understanding of Polymer Crystallization*; Reiter, G., Strobl, G., Eds.; Springer: Berlin, 2007.

(28) Wunderlich, B. *Macromolecular Physics*; Academic Press: New York, 1973, 1976, 1980; Vols. 1−3.

(29) Zhang, F.; Baralia, G.; Boborodea, A.; Bailly, C.; Nysten, B.; Jonas, A. M. *Langmuir* **2005**, *21*, 7427.

(30) Mellbring, O.; Kihlman Qiseth, S.; Krozer, A.; Lausmaa, J.; Hjertberg, T. *Macromolecules* **2001**, *34*, 7496.

(31) Baralia, G. G.; Filiâtre, C.; Nysten, B.; Jonas, A. M. *Adv. Mater.* **2007**, *19*, 4453.

(32) Stack, G. M.; Mandelkern, L.; Voigt-Martin, I. G. *Macromolecules* **1984**, *17*, 321.

(33) Israelachvili, J. N. *Intermolecular and Surface Forces*; Academic Press: San Diego, 1992.

(34) Parsegian, V. A. *Van der Waals Forces*; Cambridge University Press: New York, 2006.

(35) Tagawa, M.; Gotoh, K.; Yasukawa, A.; Ikuta, M. *Colloid Polym. Sci.* **1990**, *268*, 589.

(36) Boese, R.; Weiss, H. C.; Bläser, D. *Angew. Chem., Int. Ed.* **1999**, *38*, 988.

(37) Chevallier, V.; Petitjean, D.; Ruffier-Meray, V.; Dirand, M. *Polymer* **1999**, *40*, 5953.

(38) Butt, H. J.; Graf, K.; Kappl, M. *Physics and Chemistry of Interfaces*, 2nd ed.; Wiley-VCH: Weinheim, 2006.